

Recent astrophysical observations reproduced by a short-range correlated van der Waals-type model?

E. H. Rodrigues¹, M. Dutra^{1,2}, and O. Lourenço^{1,2}

¹*Departamento de Física, Instituto Tecnológico de Aeronáutica, DCTA, 12228-900, São José dos Campos, SP, Brazil*

²*Université de Lyon, Université Claude Bernard Lyon 1, CNRS/IN2P3, IP2I Lyon, UMR 5822, F-69622, Villeurbanne, France*

25 July 2023

ABSTRACT

We perform an improvement in a van der Waals-type model by including its effects of short-range correlations (SRC). Attractive and repulsive parts of the nucleon-nucleon interaction are assumed to be density-dependent functions, more specifically, we adopt the Carnahan–Starling (CS) method for the latter, and a suitable expression for the former in order to reproduce the structure of the Clausius (C) real gas model. The parametrizations of the resulting model, named as CCS-SRC model, are shown to be capable of reproducing the flow constraint at the high-density regime of symmetric nuclear matter for incompressibility values inside the range of $K_0 = (240 \pm 20)$ MeV. In the context of stellar matter, our findings point out a good agreement of the CCS-SRC model with recent astrophysical observational data, namely, mass-radius contours and dimensionless tidal deformability regions and values, coming from gravitational waves data related to the GW170817 and GW190425 events, and from the NASA’s Neutron star Interior Composition Explorer (NICER) mission. Furthermore, the values for the symmetry energy slope of the model (L_0) are in agreement with a recent range found for this quantity, claimed to be consistent with results reported by the updated lead radius experiment (PREX-2) collaboration. In this case, higher values of L_0 are favored, while the opposite scenario does not allow simultaneous compatibility between the model and the astrophysical data.

Key words: stars: neutron – equation of state – gravitational waves

1 INTRODUCTION

The universe is composed of many kinds of interesting structures, among them compact objects, namely, remnants of massive stars (mass bigger than six to eight times that of our sun), black holes, white dwarfs, and neutron stars (NSs). NSs are one of the densest existing objects and their internal structure is not fully known (Menezes 2021). The number of NSs is estimated to be around one billion in Milky Way, but only a few thousand have been already observed (Camenzind 2007). However, this scenario has been changing with advances in observational technologies of gravitational waves from high-frequency telescopes. Operating missions such as NASA’s Neutron star Interior Composition Explorer Mission (NICER) (Gendreau et al. 2016), and interferometers such as the Laser Interferometer Gravitational-Wave Observatory (LIGO) (Abbott et al. 2009), and the Virgo gravitational-wave detector (Accadia et al. 2012), hosted by the European Gravitational Observatory (EGO), have increased on a daily basis the number of detected objects. The fourth LIGO observation run will start in 2023 and projects a sensitivity goal of 160–190 Mpc for binary neutron star mergers, which means an increase in sensitivity of 35%, and certainly, the emergence of a large amount of new data (LIGO-Calltech 2023).

The high-density environment found in NSs makes them excellent natural laboratories for the study and application of different models based on relativistic/nonrelativistic hadronic physics. Concerning the theory used to construct such models, it is worth mentioning that there are at least two conceptions of approaching. One

of them uses the available nucleon-nucleon interactions to perform Brueckner-Hartree-Fock calculations (Ring & Schuck 2000). The second approach is based on the fitting of some many-nucleon observables, additionally using the mean-field approximation, that allows the derivation of equations of state (EoS) used to describe nuclear properties in finite (nuclei) and infinite systems (symmetric and asymmetric infinite nuclear matter) at zero and finite temperature regimes. Many studies are dedicated to implementing this method, in which nonrelativistic and relativistic hadronic models are equally applied. A particular class of hadronic models used to describe nuclear matter through the second approach takes into account relativistic effects presented by nucleons in the medium. The first version of these models was proposed in Walecka (1974) and is based on Quantum Field Theory, where a Lorentz invariant Lagrangian density is the starting point from which all thermodynamical quantities are derived.

Recently, a new type of relativistic model has been used to describe nuclear systems, such as those found in NSs. It is based on the classical van der Waals (vdW) EoS, but generalized for quantum systems also including relativity in its structure (Vovchenko et al. 2015a,b; Vovchenko 2017; Vovchenko et al. 2017). A modified version of this model was proposed in Lourenço et al. (2019) and Dutra et al. (2020) where the authors developed an approach in which both parts of the interaction, repulsive and attractive, are depending on the nuclear density. The model was verified to be consistent with some nuclear/stellar matter constraints. Here we proceed to improve such a model by including on it an important phenomenology observed

in nuclear systems, namely, the short-range correlations (SRC): effect exhibited in pairs of non-independent nucleons that emerge with high relative momentum in some nuclei such as ^{12}C , ^{27}Al , ^{56}Fe and ^{208}Pb . The effect was observed after the collision of these nuclei with highly energetic incident particles (Hen et al. 2014; CLAS Collaboration 2018, 2019; Schmidt et al. 2020; Hen et al. 2017; Duer et al. 2019) in experiments performed, for instance, at the Thomas Jefferson National Accelerator Facility (Subedi et al. 2008). We investigate how SRC impact the excluded volume model used here, and show that the improved model is in agreement with the flow constraint established in Danielewicz et al. (2002a), and also with recent astrophysical observational data provided by LIGO and Virgo Collaboration, and by the analysis of the NICER mission observations. For the comparison with these specific data, we present the results of the model concerning the mass-radius profiles and tidal deformability related to the binary neutron stars system.

Our paper is organized as follows: in Sec. 2 we present the main features of the density-dependent vdW model constructed in Lourenço et al. (2019); Dutra et al. (2020) on which our improved model is based on. Then, in Sec. 3 we develop the inclusion of SRC and show how such effects change the previous model for symmetric nuclear matter and stellar matter. For both cases, we show that important constraints are satisfied by the new excluded-volume-SRC model. Finally, in Sec. 4 we finish our study by exhibiting a brief summary of our main results, and some concluding remarks.

2 DENSITY DEPENDENT VDW MODEL APPLIED TO NUCLEAR MATTER

The idea of converting the classical vdW model into a quantum version with relativistic effects included was originally presented in Vovchenko et al. (2015a,b); Vovchenko (2017); Vovchenko et al. (2017). In principle, such a modification is enough to make the model able to describe the basic phenomenology of the nucleon-nucleon interaction, namely, attractive and repulsive parts, simulated in this approach by the correction in the ideal gas pressure, and the excluded volume, respectively. In the zero temperature regime, the authors have successfully determined numerical values for the two free constants presented in the model (a and b) by imposing $B_0 = -16$ MeV (binding energy), and $\rho_0 = 0.16 \text{ fm}^{-3}$ (saturation density) for the symmetric nuclear matter (SNM) case, in which the proton fraction is $y_p = 0.5$. This procedure lead to $a \sim 329 \text{ MeV fm}^3$ and $b \sim 3.42 \text{ fm}^3$. Even with the saturation point ensured, the simplest version of the vdW model applied to nuclear matter still contains some issues, such as the value obtained for incompressibility at the saturation density, $K_0 \sim 760$ MeV. The modification of the excluded volume mechanism implemented, namely, from the traditional one to the Carnahan-Starling (CS) procedure (Carnahan & Starling 1969), decreases this number to $K_0 \sim 330$ MeV. However, this value is still not inside the empirical range of $K_0 = (240 \pm 20)$ MeV (Shlomo et al. 2006; Garg & Colò 2018), or the one given in Stone et al. (2014): $K_0 = (250 - 315)$ MeV. Despite that, this model and its variations, such as the Clausius-CS model, are capable of reproducing lattice data at finite temperature regime (Vovchenko 2017).

In Lourenço et al. (2019) a generalization of the vdW model was proposed. More specifically, possible density dependence in the attractive contribution was taken into account. For the term containing the excluded volume, the aforementioned CS procedure was used as well. In summary, the EoS for energy density and pressure are given,

respectively, by

$$\epsilon(\rho, y_p) = [1 - \rho\mathcal{B}(\rho)] \left(\epsilon_{\text{kin}}^{\star p} + \epsilon_{\text{kin}}^{\star n} \right) - \rho^2 \mathcal{A}(\rho) + d(2y_p - 1)^2 \rho^2, \quad (1)$$

and

$$p(\rho, y_p) = p_{\text{kin}}^{\star p} + p_{\text{kin}}^{\star n} - \rho^2 \mathcal{A}(\rho) + \rho \Sigma(\rho, y_p) + d(2y_p - 1)^2 \rho^2, \quad (2)$$

with $\Sigma(\rho, y_p) = \rho \mathcal{B}'(P_{\text{kin}}^{\star p} + P_{\text{kin}}^{\star n}) - \rho^2 \mathcal{A}'$ being the rearrangement term with $\mathcal{A}' \equiv d\mathcal{A}/d\rho$, and $\mathcal{B}' \equiv d\mathcal{B}/d\rho$. The kinetic contributions are

$$\epsilon_{\text{kin}}^{\star p,n} = \frac{\gamma}{2\pi^2} \int_0^{k_F^{\star p,n}} dk k^2 \sqrt{k^2 + M^2}, \quad (3)$$

and

$$p_{\text{kin}}^{\star p,n} = \frac{\gamma}{6\pi^2} \int_0^{k_F^{\star p,n}} dk k^4. \quad (4)$$

The Fermi momentum of the nucleon of mass $M = 939$ MeV and degeneracy factor $\gamma = 2$ is related to its respective density as $k_F^{\star p,n} = (6\pi^2 \rho_{p,n}^{\star} / \gamma)^{1/3}$, where

$$\rho_p^{\star} = \frac{y_p \rho}{1 - \rho\mathcal{B}(\rho)} = \frac{\rho_p}{1 - \rho\mathcal{B}(\rho)}, \quad (5)$$

$$\rho_n^{\star} = \frac{(1 - y_p)\rho}{1 - \rho\mathcal{B}(\rho)} = \frac{\rho_n}{1 - \rho\mathcal{B}(\rho)}.$$

Finally, the density-dependent functions \mathcal{A} and \mathcal{B} are

$$\mathcal{A}(\rho) = \frac{a}{(1 + b\rho)^n}, \quad (6)$$

and

$$\mathcal{B}(\rho) = \frac{1}{\rho} - \frac{1}{\rho} \exp \left[-\frac{b\rho}{4} \frac{\left(4 - \frac{3b\rho}{4}\right)}{\left(1 - \frac{b\rho}{4}\right)^2} \right], \quad (7)$$

with this last one determined through the CS approach for the repulsive interaction (excluded volume). It is worth noticing that from this general structure, it is possible to recover the other real gases studied in Vovchenko (2017) for the $y_p = 0.5$ case, as for instance the vdW-CS model itself, by using $n = 0$, and the Clausius-CS one, for which $n = 1$. The traditional versions of these models regarding the excluded volume method are obtained by making $\mathcal{B}(\rho) \rightarrow b$ in addition. Another formulation involving a vdW model in which induced surface tension is taken into account was implemented in Sagun et al. (2018); Bugaev et al. (2019).

This new model, named the density-dependent vdW (DD-vdW) model, has shown to preserve causality in a density regime capable of producing mass-radius diagrams consistent with data obtained from the PSR J0348+0432 pulsar (Antoniadis et al. 2013), as well as those from the GW170817 neutron-star merger event. It is also compatible with the flow constraint established in Danielewicz et al. (2002a). The four free parameters (a , b , d and n) are determined by imposing specific values for ρ_0 , B_0 , K_0 and J (symmetry energy at ρ_0). Furthermore, it also produces some clear correlations in SNM as one can see in Dutra et al. (2020).

3 SHORT-RANGE CORRELATIONS: CCS-SRC MODEL

The inclusion of SRC in hadronic models is performed by modifying the single-nucleon momentum distributions, from the usual

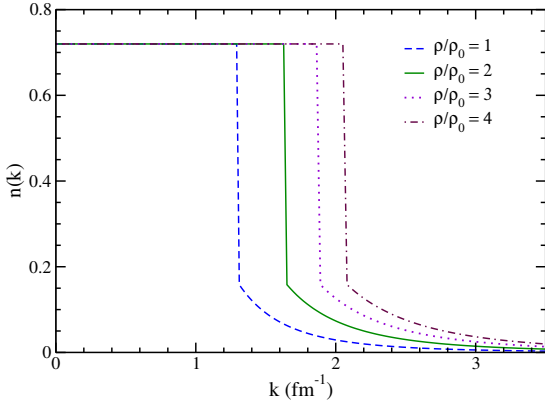


Figure 1. Momentum distribution with HMT included for symmetric nuclear matter. Curves for $\rho/\rho_0 = 1, 2, 3$ and 4 , with $\rho_0 = 0.15 \text{ fm}^{-3}$.

Fermi step functions to those encompassing the high-momentum tail (HMT) that read

$$n_{p,n}(k) = \begin{cases} \Delta_{p,n}, & 0 < k < k_F^{p,n} \\ C_{p,n} \frac{(k_F^{p,n})^4}{k^4}, & k_F^{p,n} < k < \phi_{p,n} k_F^{p,n}, \end{cases} \quad (8)$$

with $\Delta_{p,n} = 1 - 3C_{p,n}(1 - 1/\phi_{p,n})$, $C_p = C_0[1 - C_1(1 - 2y_p)]$, $C_n = C_0[1 + C_1(1 - 2y_p)]$, $\phi_p = \phi_0[1 - \phi_1(1 - 2y_p)]$ and $\phi_n = \phi_0[1 + \phi_1(1 - 2y_p)]$. The values $C_0 = 0.161$, $C_1 = -0.25$, $\phi_0 = 2.38$, and $\phi_1 = -0.56$ are determined (Cai & Li 2015, 2016a,b) by taking experimental data concerning $d(e, e', p)$ and two-nucleon knockout reactions, medium-energy photonuclear absorption, as well as by using the normalization condition

$$\frac{1}{\pi^2} \int_0^\infty dk k^2 n_{p,n}(k) = \rho_{p,n} = \frac{(k_F^{p,n})^3}{3\pi^2}. \quad (9)$$

Furthermore, the fraction of nucleons in the HMT given by $x^{\text{HMT}} = 3C_{p,n}(1 - \phi_{p,n}^{-1})$ is also used in this determination, namely, $x_{\text{SNM}}^{\text{HMT}} = 28\%$ and $x_{\text{PNM}}^{\text{HMT}} = 1.5\%$: numbers obtained for symmetric nuclear matter and pure neutron matter, respectively (Cai & Li 2015, 2016a,b). In Fig. 1 we depict the $n(k)$ distribution in SNM for some values of ρ/ρ_0 .

Recently, some papers have explored possible modifications in Eq. (8) and their consequences. In Cai & Li (2022), for instance, it was studied the effect of generalizing $n_{p,n}(k)$ to arbitrary dimensions. In Guo et al. (2021) on the other hand, the authors investigated three different shapes for the SRC HMT, namely, proportional to k^4 , k^6 , and k^9 . The analysis performed in this paper is based on hard photons emissions due to the reactions $^{14}\text{N}+^{12}\text{C}$ and $^{48}\text{Ca}+^{124}\text{Se}$ at beam energies around the Fermi energy. From the reactions, they analyzed the yields, angular distribution, and energy spectra of the hard photons, leading them to important conclusions. The first is related to the yields, which increase equally for all different powers of k . The second is that the shape of the HMT does not affect the angular distribution of the produced hard photons. In this way, if one looks only at the yields or at the angular distribution, the shape seems not to be relevant. The two first conclusions make the third one the most meaningful. The authors have calculated the effects of the HMT shape in the hard photons spectra, finding that this effect is considerable and should not be ignored. The effects are greater as greater are the energy of the photons.

Here we use the expression given in Eq. (8) adapted to the case in which excluded volume effects are implemented in the system,

namely, taking $k_F^{p,n} \rightarrow k_F^{*p,n}$, in order to generate new EoS for the vdW-type model presented before. This procedure leads to generalized thermodynamical quantities, such as energy density and pressure, given respectively by,

$$\epsilon(\rho, y_p) = [1 - \rho\mathcal{B}(\rho)] \left[\epsilon_{\text{kin(SRC)}}^{*p} + \epsilon_{\text{kin(SRC)}}^{*n} \right] - \rho^2 \mathcal{A}(\rho) + d(2y_p - 1)^2 \rho^2, \quad (10)$$

and

$$p(\rho, y_p) = p_{\text{kin(SRC)}}^{*p} + p_{\text{kin(SRC)}}^{*n} - \rho^2 \mathcal{A}(\rho) + \rho \Sigma_{\text{SRC}}(\rho, y_p) + d(2y_p - 1)^2 \rho^2, \quad (11)$$

where

$$\Sigma_{\text{SRC}}(\rho, y_p) = \rho \mathcal{B}' \left[p_{\text{kin(SRC)}}^{*p} + p_{\text{kin(SRC)}}^{*n} \right] - \rho^2 \mathcal{A}', \quad (12)$$

and with modified kinetic terms written as

$$\epsilon_{\text{kin(SRC)}}^{*p,n} = \frac{\gamma \Delta_{p,n}}{2\pi^2} \int_0^{k_F^{*p,n}} dk k^2 \sqrt{k^2 + M^2} + \frac{\gamma C_{p,n} (k_F^{*p,n})^4}{2\pi^2} \int_{k_F^{*p,n}}^{\phi_{p,n} k_F^{*p,n}} dk \frac{\sqrt{k^2 + M^2}}{k^2}, \quad (13)$$

and

$$p_{\text{kin(SRC)}}^{*p,n} = \frac{\gamma \Delta_{p,n}}{6\pi^2} \int_0^{k_F^{*p,n}} dk k^4 \sqrt{k^2 + M^2} + \frac{\gamma C_{p,n} (k_F^{*p,n})^4}{6\pi^2} \int_{k_F^{*p,n}}^{\phi_{p,n} k_F^{*p,n}} dk \frac{k^4}{\sqrt{k^2 + M^2}}, \quad (14)$$

with the normalization condition, now taken as $\int_0^\infty n_{p,n}(k) k^2 dk = \rho_{p,n}^*$, giving the same numbers for C_0 , C_1 , ϕ_0 , and ϕ_1 . Furthermore, we consider the CS excluded volume mechanism for the function $\mathcal{B}(\rho)$, Eq. (7). In the case of the attractive density-dependent function $\mathcal{A}(\rho)$, we make $n = 1$ and $b \rightarrow c$ in Eq. (6), namely,

$$\mathcal{A}(\rho) = \frac{a}{1 + c\rho}. \quad (15)$$

By doing so, we actually assume the three parameters Clausius-CS model applied to the nuclear matter as shown in Vovchenko (2017); Vovchenko et al. (2018), but also generalized to include SRC effects. Hereafter we name it as CCS-SRC model. The four free parameters of the model, a , b , c and d , are determined by imposing $\rho_0 = 0.15 \text{ fm}^{-3}$, $B_0 = -16 \text{ MeV}$, $J = E_{\text{sym}}(\rho_0) = 32 \text{ MeV}$, and some values for $K_0 = K(\rho_0, y_p = \frac{1}{2})$. The expression for the incompressibility in SNM is given by

$$K(\rho) = 9 \frac{\partial P}{\partial \rho} \Big|_{y_p = \frac{1}{2}} = 9[\Sigma_{\text{SRC}}(\rho) + \rho \Sigma'_{\text{SRC}}(\rho)] + \frac{1 + \mathcal{B}'\rho^2}{[1 - \mathcal{B}(\rho)\rho]^2} K_{\text{kin(SRC)}}^* - 9\rho[2\mathcal{A}(\rho) + \mathcal{A}'\rho], \quad (16)$$

with $\Sigma_{\text{SRC}}(\rho) = \Sigma_{\text{SRC}}(\rho, y_p = 1/2)$,

$$\Sigma'_{\text{SRC}}(\rho) = (\mathcal{B}''\rho + \mathcal{B}') p_{\text{kin(SRC)}}^* + \frac{(1 + \mathcal{B}'\rho^2)\mathcal{B}'\rho}{9[1 - \mathcal{B}(\rho)\rho]^2} K_{\text{kin(SRC)}}^* - \mathcal{A}''\rho^2 - 2\mathcal{A}'\rho, \quad (17)$$

$$\begin{aligned}
 K_{\text{kin(SRC)}}^* &= \frac{3\Delta k_F^{*2}}{\sqrt{k_F^{*2} + M^2}} \\
 &+ 3C_0 k_F^{*2} \left[\frac{\phi_0}{\sqrt{\phi_0^2 k_F^{*2} + M^2}} - \frac{1}{\sqrt{k_F^{*2} + M^2}} \right. \\
 &\left. + \frac{4}{k_F^*} \ln \left(\frac{\phi_0 k_F^* + \sqrt{\phi_0^2 k_F^{*2} + M^2}}{k_F^* + \sqrt{k_F^{*2} + M^2}} \right) \right], \quad (18)
 \end{aligned}$$

and $\Delta = 1 - 3C_0(1 - 1/\phi_0)$. For $P_{\text{kin(SRC)}}^*$ shown in Eq. (17), we use the expression given in Eq. (14) with $k_F^{*p,n}$ replaced by k_F^* and $\gamma = 4$.

The symmetry energy reads

$$\begin{aligned}
 E_{\text{sym}}(\rho) &= \frac{1}{8} \frac{\partial^2(\epsilon/\rho)}{\partial y_p^2} \Big|_{y_p=\frac{1}{2}} = \frac{k_F^{*2}}{6E_F^*} \left[1 - 3C_0 \left(1 - \frac{1}{\phi_0} \right) \right] \\
 &- 3C_0 E_F^* \left[C_1 \left(1 - \frac{1}{\phi_0} \right) + \frac{\phi_1}{\phi_0} \right] \\
 &- \frac{9M^4}{8k_F^{*3}} \frac{C_0 \phi_1 (C_1 - \phi_1)}{\phi_0} \left[\frac{2k_F^*}{M} \left(1 + \frac{k_F^{*2}}{M^2} \right)^{3/2} \right. \\
 &\left. - \frac{k_F^*}{M} \sqrt{1 + \frac{k_F^{*2}}{M^2}} - \text{arcsinh} \left(\frac{k_F^*}{M} \right) \right] \\
 &+ \frac{2C_0 k_F^* (6C_1 + 1)}{3} \left[\sqrt{1 + \frac{M^2}{k_F^{*2}}} - \sqrt{1 + \frac{M^2}{k_F^{*2} \phi_0^2}} \right. \\
 &\left. + \text{arcsinh} \left(\frac{k_F^* \phi_0}{M} \right) - \text{arcsinh} \left(\frac{k_F^*}{M} \right) \right] \\
 &+ \frac{3C_0 k_F^*}{2} \left[\frac{4E_F^*}{9k_F^*} - \frac{k_F^*}{9E_F^*} + \frac{1}{9} (3\phi_1 + 1)^2 \left(\frac{k_F^* \phi_0}{F_F^*} - \frac{2F_F^*}{k_F^* \phi_0} \right) \right. \\
 &\left. + \frac{2F_F^* (3\phi_1 - 1)}{9k_F^* \phi_0} \right] \\
 &+ \frac{C_0 (3C_1 + 4)}{3} \left[\frac{F_F^* (3\phi_1 + 1)}{\phi_0} - E_F^* \right] + d\rho, \quad (19)
 \end{aligned}$$

with $E_F^* = \sqrt{k_F^{*2} + M^2}$ and $F_F^* = \sqrt{\phi_0^2 k_F^{*2} + M^2}$.

It is worth mentioning that Eq. (16) reduces to that one related to the DD-vdW model (Lourenço et al. 2019) when SRC are turned off, by taking $\phi_0 = 1$ and $\phi_1 = 0$, and when Eq. (6) is used instead of Eq. (15). With regard to the symmetry energy, notice that its kinetic part, given by $E_{\text{sym}}^{\text{kin}}(\rho) = E_{\text{sym}}(\rho) - d\rho$, is exactly the same presented in Cai & Li (2016a) for the case in which no excluded volume effects are considered in the system, i.e., for $k_F^* = k_F$. Furthermore, we find $E_{\text{sym}}^{\text{kin}}(\rho_0) = -14.7$ MeV for the kinetic part of the symmetry energy at the saturation density. This value is compatible with respective numbers obtained in Cai & Li (2016a) from a nonlinear relativistic mean-field (RMF) model, and from a nonrelativistic calculation, both including SRC effects.

For the sake of completeness, we also investigate how the symmetry energy and its slope, obtained through $L = 3\rho(\partial E_{\text{sym}}/\partial\rho)$, correlates with each other (both quantities evaluated at the saturation density: J and $L_0 = L(\rho_0)$). Such a relationship is depicted in Fig. 2. From the figure, it is verified a strong linear correlation between these quantities, in accordance with many other approaches performed in the literature, as can be seen, in Drischler et al. (2020); Li et al. (2021); Santos et al. (2015), for example. Another feature exhibited in the figure is that SRC significantly increases the values of L_0 for

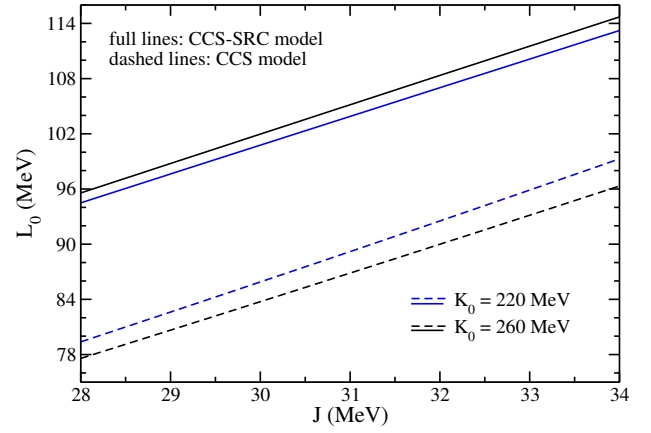


Figure 2. L_0 as a function of J for the CCS model with (full lines) and without (dashed lines) SRC included. Curves constructed by using $\rho_0 = 0.15 \text{ fm}^{-3}$, $B_0 = -16$ MeV.

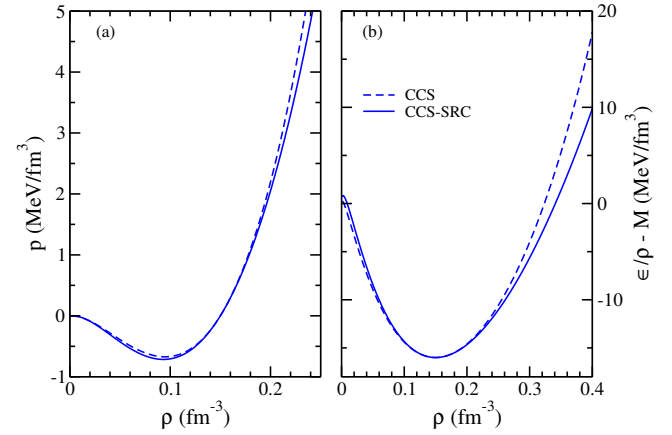


Figure 3. CCS model with (full lines) and without (dashed lines) SRC included: (a) pressure and (b) energy per particle as a function of the density. Curves for symmetric nuclear matter with $\rho_0 = 0.15 \text{ fm}^{-3}$, $B_0 = -16$ MeV, and $K_0 = 240$ MeV.

the same J . It is also observed that there is no big impact in L_0 for K_0 changing in the range of $K_0 = (240 \pm 20)$ MeV.

3.1 Applications in SNM and stellar matter

We show in Figs. 3a and 3b the effect of the SRC applied to the CCS-SRC model in the energy per particle and pressure of the system in SNM. From these figures, we notice that SRC mainly affects such thermodynamical quantities especially for densities greater than 0.2 fm^{-3} , approximately. In this case, it is important to verify the results of the model regarding the high-density regime. For this purpose, we also investigate how it behaves against the so-called flow constraint. It is based on the study performed in Danielewicz et al. (2002b) in which limits on the pressure of SNM (zero temperature case) at high densities were established from experimental data related to the motion of ejected matter in energetic nucleus–nucleus collisions, more specifically, particle flow in the collisions of ^{197}Au nucleus at incident kinetic energy per nucleon running from about 0.15 GeV to 10 GeV. The comparison of the model with this constraint is displayed in Fig. 4. It is verified that parametrizations of the CCS-SRC model constructed by fixing K_0 in the range of

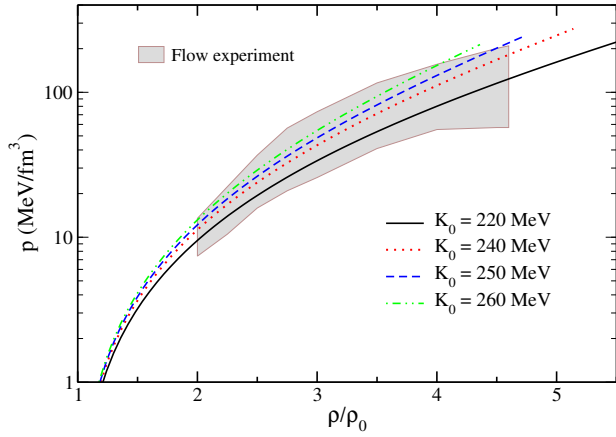


Figure 4. Pressure versus ρ/ρ_0 for different parametrizations of the CCS-SRC model. Curves for symmetric nuclear matter with $\rho_0 = 0.15 \text{ fm}^{-3}$ and $B_0 = -16 \text{ MeV}$. Band: flow constraint extracted from (Danielewicz et al. 2002a).

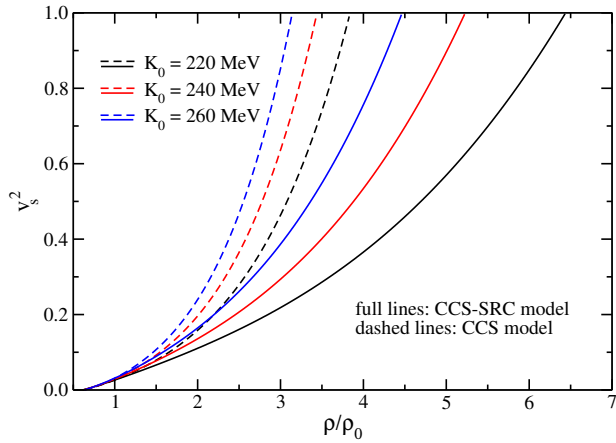


Figure 5. Squared sound velocity as a function of ρ/ρ_0 for different parametrizations of the CCS model with (full lines) and without (dashed lines) SRC included. Curves for symmetric nuclear matter with $\rho_0 = 0.15 \text{ fm}^{-3}$ and $B_0 = -16 \text{ MeV}$.

$K_0 = (240 \pm 20) \text{ MeV}$ (Garg & Colò 2018) are completely in agreement with the band provided by the flow constraint. All these curves were generated in a density range that ensures causality to the system. In the case of excluded volume models, like the one we are presenting here, nucleons are treated as finite-size objects and therefore a suitable Lorentz contraction should be taken into account for relativistic frameworks in order to avoid causality violation for any density (Bugaev 2008). An alternative to this procedure is the implementation of the CS excluded volume treatment, since this mechanism effectively produces an excluded volume depending on the density, more specifically, as a decreasing function. In the case of the model proposed in this work, we verify that SRC moves the density in which causality is broken to higher values in comparison with the model without this phenomenology implemented. This feature is observed in Fig. 5.

We also investigate the capability of the CCS-SRC model in describing stellar matter in general, and some recent astrophysical observations in particular. In order to do that, it is necessary to solve the Tolman-Oppenheimer-Volkoff (TOV) equations (Tolman 1939; Oppenheimer & Volkoff 1939), given by $dP(r)/dr = -[\varepsilon(r) + P(r)][m(r) + 4\pi r^3 P(r)]/r^2 g(r)$ and $dm(r)/dr = 4\pi r^2 \varepsilon(r)$,

where $g(r) = 1 - 2m(r)/r$. The solution of these equations is constrained to $P(0) = P_c$ (central pressure) and $m(0) = 0$, with the conditions $P(R) = 0$ and $m(R) = M_{\text{NS}}$ satisfied at the star surface. Here R defines the radius of the respective neutron star of mass M_{NS} . We impose the NS core as described by the EoS obtained from the CCS-SRC model. For the outer crust, on the other hand, we use the EoS constructed by Baym, Pethick, and Sutherland (BPS) (Baym et al. 1971) in a density range of $6.3 \times 10^{-12} \text{ fm}^{-3} \leq \rho_{\text{outer}} \leq 2.5 \times 10^{-4} \text{ fm}^{-3}$. Finally, for the inner crust of the NS, we use the polytropic form of $P(\varepsilon) = \alpha + \beta \varepsilon^{4/3}$ from $2.5 \times 10^{-4} \text{ fm}^{-3}$ to the transition density, in our case obtained through the thermodynamical method (Xu et al. 2009b; Gonzalez-Boquera et al. 2019; Xu et al. 2009a).

The total energy density and total pressure of the system composed of protons, neutrons, electrons, and muons are written as

$$\varepsilon = \varepsilon + \frac{\mu_e^4}{4\pi^2} + \frac{1}{\pi^2} \int_0^{\sqrt{\mu_\mu^2(\rho_e) - m_\mu^2}} dk k^2 (k^2 + m_\mu^2)^{1/2} \quad (20)$$

and

$$P = p + \frac{\mu_e^4}{12\pi^2} + \frac{1}{3\pi^2} \int_0^{\sqrt{\mu_\mu^2 - m_\mu^2}} dk k^4 \frac{1}{(k^2 + m_\mu^2)^{1/2}}, \quad (21)$$

where, by chemical equilibrium and charge neutrality conditions, both imposed in an NS, one has $\mu_n - \mu_p = \mu_e$ and $\rho_p - \rho_e = \rho_\mu$, with $\mu_e = (3\pi^2 \rho_e)^{1/3}$, $\rho_\mu = [(\mu_\mu^2 - m_\mu^2)^{3/2}]/(3\pi^2)$, and $\mu_\mu = \mu_e$, for $m_\mu = 105.7 \text{ MeV}$ (muon mass) and massless electrons. ε , and p are determined from the CCS-SRC model, as well as the chemical potentials for, namely,

$$\begin{aligned} \mu_{p,n} &= \frac{\partial \varepsilon}{\partial \rho_{p,n}} = \Delta_{p,n} \mu_{\text{kin}}^{\star p,n} + \mu_{\text{kin(SRC)}}^{\star p,n} \\ &+ \mathcal{B}(\rho) [P_{\text{kin(SRC)}}^{\star p} + P_{\text{kin(SRC)}}^{\star n}] \\ &+ \Sigma_{\text{SRC}}(\rho, y_p) - 2\mathcal{A}(\rho)\rho \pm 2d(2y_p - 1)\rho \end{aligned} \quad (22)$$

for protons (upper sign) and neutrons (lower sign), with

$$\begin{aligned} \mu_{\text{kin(SRC)}}^{\star p,n} &= 3C_{p,n} \left[\mu_{\text{kin}}^{\star p,n} - \frac{(\phi_{p,n}^2 k_{Fp,n}^{\star 2} + M^2)^{1/2}}{\phi_{p,n}} \right] \\ &+ 4C_{p,n} k_{Fp,n}^{\star} \ln \left[\frac{\phi_{p,n}^2 k_{Fp,n}^{\star 2} + (\phi_{p,n}^2 k_{Fp,n}^{\star 2} + M^2)^{1/2}}{k_{Fp,n}^{\star} + (k_{Fp,n}^{\star 2} + M^2)^{1/2}} \right], \end{aligned} \quad (23)$$

and $\mu_{\text{kin}}^{\star p,n} = (k_{Fp,n}^{\star 2} + M^2)^{1/2}$. Notice that Eqs. (22) reduce to the chemical potentials of the DD-vdW model when SRC are turned off ($\phi_0 = 1$ and $\phi_1 = 0$ case). Furthermore, in the case of no excluded volume implemented in the model, i.e., for $\mathcal{B}(\rho) \rightarrow 0$, the first two terms of Eqs. (22) become identical to ones related to the relativistic model studied in Souza et al. (2020), for $M \rightarrow M^*$, see Eq. 6 to 8 of that reference.

Before presenting the outcomes of the model concerning the mass-radius diagrams, we first discuss the effect of SRC in the EoS used as input to the TOV equations, by analyzing the outcomes presented in Fig. 6. As already mentioned, SRC move the break of causality to higher densities, or equivalently, to higher energy densities in the case of the data shown in the figure. Moreover, one can also notice that SRC make softer the EoS since the pressure is lower for the same value of ε in comparison with the case in which no SRC are included. This is not the case for RMF models that present quartic interaction in the vector field ω_μ , i.e., a term given by $C_\omega (\omega_\mu \omega^\mu)^2$ in its Lagrangian density, where C_ω is a constant free parameter,

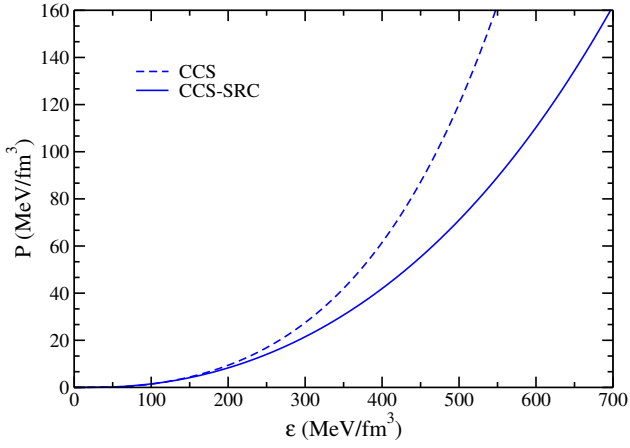


Figure 6. Total pressure vs total energy for the CCS model with (full lines) and without (dashed lines) SRC included. Curves for stellar matter with $\rho_0 = 0.15 \text{ fm}^{-3}$, $B_0 = -16 \text{ MeV}$, $K_0 = 240 \text{ MeV}$, and $J = 32 \text{ MeV}$.

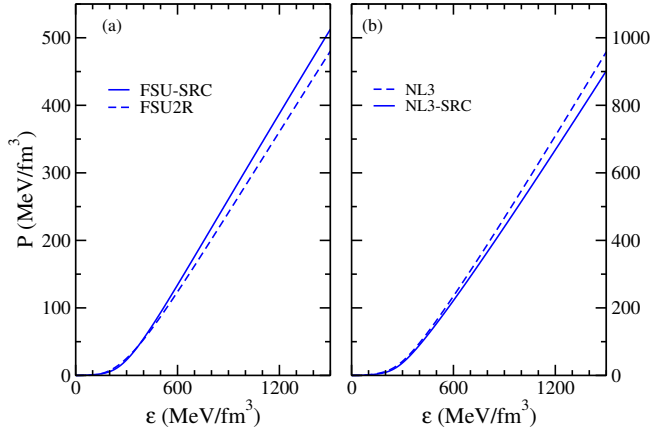


Figure 7. Total pressure as a function of total energy density (stellar matter) for the (a) FSU and (b) NL3 parametrizations with (full lines) and without (dashed lines) SRC included.

namely (Li et al. 2008; Dutra et al. 2014),

$$\begin{aligned}
 \mathcal{L} = & \bar{\psi}(i\gamma^\mu \partial_\mu - M)\psi + g_\sigma \bar{\psi}\psi\bar{\sigma} - g_\omega \bar{\psi}\gamma^\mu\omega_\mu\psi \\
 & - \frac{g_\rho}{2}\bar{\psi}\gamma^\mu\vec{\rho}_\mu\vec{\tau}\psi + \frac{1}{2}(\partial^\mu\sigma\partial_\mu\sigma - m_\sigma^2\sigma^2) - \frac{A}{3}\sigma^3 - \frac{B}{4}\sigma^4 \\
 & - \frac{1}{4}F^{\mu\nu}F_{\mu\nu} + \frac{1}{2}m_\omega^2\omega_\mu\omega^\mu + C_\omega(\omega_\mu\omega^\mu)^2 - \frac{1}{4}\vec{B}^{\mu\nu}\vec{B}_{\mu\nu} \\
 & + \frac{1}{2}\alpha'_3 g_\omega^2 g_\rho^2 \omega_\mu\omega^\mu \vec{\rho}_\mu\vec{\rho}^\mu + \frac{1}{2}m_\rho^2 \vec{\rho}_\mu\vec{\rho}^\mu. \quad (24)
 \end{aligned}$$

For models with this structure, it is verified that SRC make stiffer the EoS (the pressure is higher for the same energy density). For instance, we display in Fig. 7a this finding for the FSU2R parametrization (Tolos et al. 2017) with and without SRC. For the construction of these curves, the bulk parameters were kept the same for both approaches (with and without SRC) as well as the value of the constant C_ω , the procedure also adopted in Cai & Li (2016a); Souza et al. (2020). Despite this result, it is worth mentioning that SRC can also soften the EoS even for RMF models. This is the case for parametrizations with $C_\omega = 0$. As an example, we plot in Fig. 7b total pressure as a function of total energy density for the NL3 (Lalazissis et al. 1997; Silva et al. 2008) parametrization, for which there is no quartic self-interaction in the repulsive vector channel. As we see, the effect of

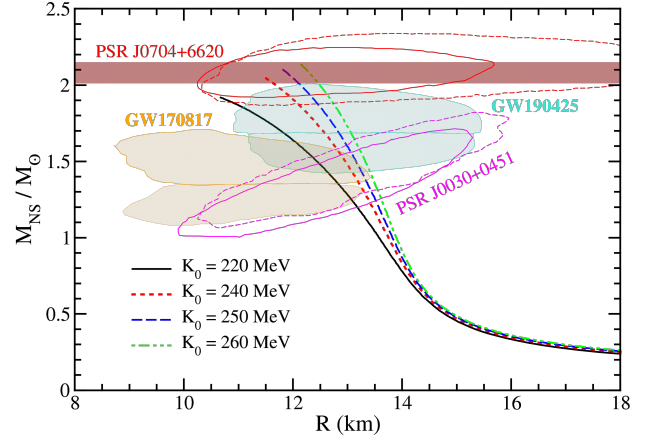


Figure 8. Mass-radius diagrams constructed from the CCS-SRC model with different values of K_0 . The contours are related to data from the NICER mission, namely, PSR J0030+0451 (Riley et al. 2019; Miller et al. 2019) and PSR J0740+6620 (Riley et al. 2021; Miller et al. 2021), the GW170817 (Abbott et al. 2017, 2018) and the GW190425 events (Abbott et al. 2020), all of them at 90% credible level. The red horizontal lines are also related to the PSR J0740+6620 pulsar (Fonseca et al. 2021).

including SRC is exactly the opposite of that verified for the FSU2R parametrization, but the same as the one presented by the CCS-SRC model. It is known that hadronic models with stiffer EoS produce more massive neutron stars. This is a direct consequence of introducing SRC in RMF models with $C_\omega \neq 0$, as verified in Cai & Li (2016a); Souza et al. (2020); Lourenço et al. (2022); Lourenço et al. (2022), for instance. For the case of models with softer EoS, the opposite is expected. In our case, despite SRC generating softer EoS, we still find possible parametrizations of the CCS-SRC model capable of reproducing recent astrophysical observational data, as presented in Fig. 8. Notice that the model produces mass-radius diagrams in agreement with the following astrophysical constraints: gravitational waves data related to the GW170817 (Abbott et al. 2017, 2018) and GW190425 (Abbott et al. 2020) events, some of them provided by the LIGO and Virgo Collaboration; data from the NICER mission regarding the pulsars PSR J0030+0451 (Riley et al. 2019; Miller et al. 2019) and PSR J0740+6620 (Riley et al. 2021; Miller et al. 2021); and data from the latter pulsar extracted from Fonseca et al. (2021).

For the sake of completeness, we present in Fig. 9b the plot of the stellar mass as a function of the central density for the different CCS-SRC parametrizations used here. In addition, we show in Fig. 9a the squared sound velocity for beta-equilibrated matter, $v_s^2 = \partial P / \partial \varepsilon$, also as a function of the density. By comparing the results of both panels, it is possible to confirm that a break of causality is not observed for the configurations of the stars generated by the model.

We also verify the results obtained through the model with regard to the dimensionless tidal deformability. This quantity is defined as $\Lambda = 2k_2 / (3C^5)$, with $C = M_{\text{NS}} / R$, and the second Love number given by

$$\begin{aligned}
 k_2 = & \frac{8C^5}{5}(1-2C)^2[2+2C(y_R-1)-y_R] \\
 & \times \left\{ 2C[6-3y_R+3C(5y_R-8)] \right. \\
 & + 4C^3[13-11y_R+C(3y_R-2)+2C^2(1+y_R)] \\
 & \left. + 3(1-2C)^2[2-y_R+2C(y_R-1)]\ln(1-2C) \right\}^{-1}, \quad (25)
 \end{aligned}$$

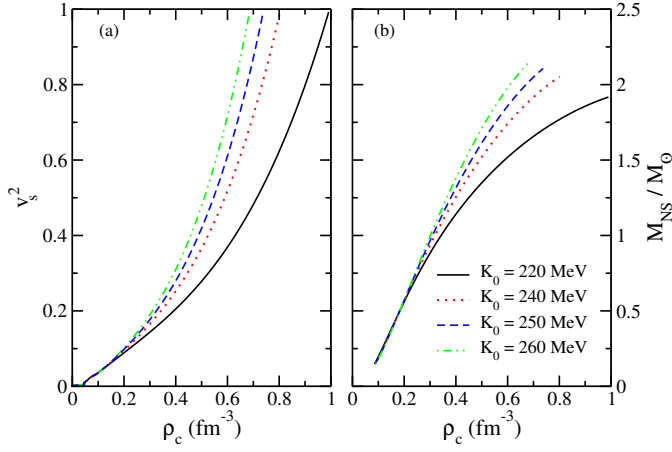


Figure 9. (a) Squared sound velocity for beta-equilibrated matter, and (b) stellar mass in units of M_\odot , both as a function of the central density for the CCS-SRC model. All curves constructed by using $\rho_0 = 0.15 \text{ fm}^{-3}$, $B_0 = -16 \text{ MeV}$, $J = 32 \text{ MeV}$, and different values of K_0 .

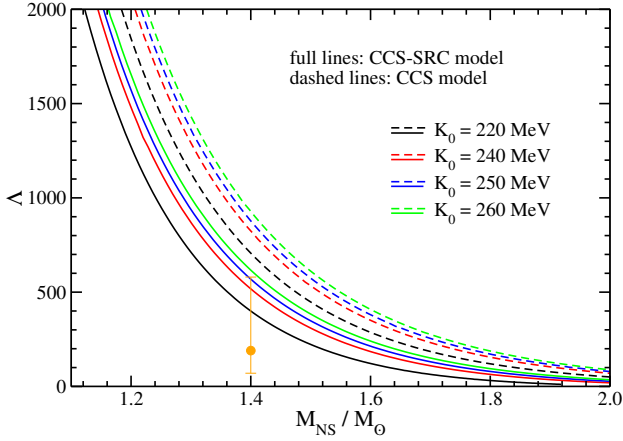


Figure 10. Λ versus M_{NS}/M_\odot for the CCS model with $\rho_0 = 0.15 \text{ fm}^{-3}$, $B_0 = -16 \text{ MeV}$, $J = 32 \text{ MeV}$, and different values of K_0 with (full lines) and without (dashed lines) SRC included. Full circle with error bars: result of $\Lambda_{1,4} = 190^{+390}_{-120}$ obtained in (Abbott et al. 2018).

with $y_R = y(R)$. The quantity $y(r)$ is determined from the solution of the differential equation $r(dy/dr) + y^2 + yF(r) + r^2Q(r) = 0$, solved simultaneously with the TOV ones. The expressions for the functions $F(r)$ and $Q(r)$ are

$$F(r) = \frac{1 - 4\pi r^2 [\epsilon(r) - p(r)]}{g(r)}, \quad (26)$$

$$Q(r) = \frac{4\pi}{g(r)} \left[5\epsilon(r) + 9p(r) + \frac{\epsilon(r) + p(r)}{v_s^2(r)} - \frac{6}{4\pi r^2} \right] - 4 \left[\frac{m(r) + 4\pi r^3 p(r)}{r^2 g(r)} \right]^2, \quad (27)$$

with $v_s^2(r) = \partial p(r)/\partial \epsilon(r)$ being the squared sound velocity (Postnikov et al. 2010; Hinderer 2008; Damour & Nagar 2010; Binnington & Poisson 2009). We show the results concerning Λ in Fig. 10. From this figure, one notices that the inclusion of SRC in the system favors the model to attain the constraint of $\Lambda_{1,4} = 190^{+390}_{-120}$ (Abbott et al. 2018) for parametrizations with $K_0 = (240 \pm 20) \text{ MeV}$. For the model presented here, it is also clear that the inclusion of SRC systemat-

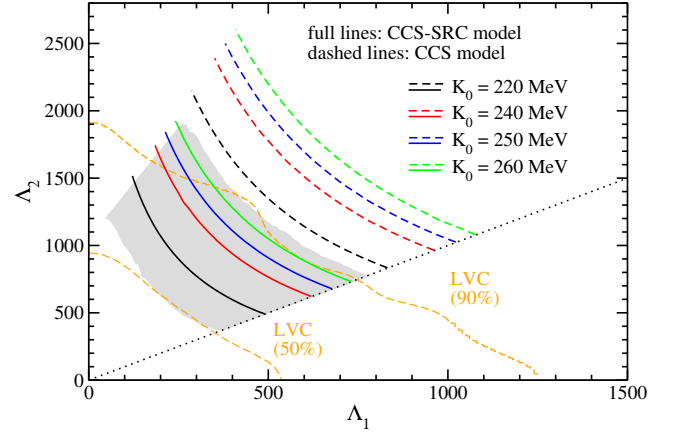


Figure 11. Λ_2 versus Λ_1 for the CCS model with $\rho_0 = 0.15 \text{ fm}^{-3}$, $B_0 = -16 \text{ MeV}$, $J = 32 \text{ MeV}$, and different values of K_0 with (full lines) and without (dashed lines) SRC included. The orange dashed lines correspond to the 90% and 50% confidence limits given by the LIGO and Virgo Collaboration (LVC) (Abbott et al. 2018). The gray band represents the results obtained through the relativistic mean field models studied in (Lourenço et al. 2019).

ically decreases Λ in all cases. The physical reason for this effect comes from the fact that SRC soften the EoS, as already discussed. In this case, the NS radius is also reduced by these correlations, and due to the relation given by $\Lambda \sim R^\alpha$, verified in different hadronic models for a $1.4 M_\odot$ star for instance (Lourenço et al. 2019; Lourenço et al. 2020), it is straightforward to conclude that Λ decreases with the radius decreasing. For the CCS model, this decrease makes the model compatible with the astrophysical data analyzed. Finally, we plot in Fig. 11 the tidal deformabilities Λ_1 and Λ_2 of the binary neutron stars system with component masses m_1 and m_2 ($m_1 > m_2$), related to the GW170817 event, and taking into account the range for m_1 given by $1.365 \leq m_1/M_\odot \leq 1.60$ (Abbott et al. 2017). The mass of the companion star m_2 , is obtained from the relationship between m_1 , m_2 , and the chirp mass, that reads

$$\mathcal{M}_c = \frac{(m_1 m_2)^{3/5}}{(m_1 + m_2)^{1/5}}, \quad (28)$$

and is fixed at the observed value of $1.188 M_\odot$, according to Abbott et al. (2017). Upper and lower orange dashed lines correspond to the 90% and 50% confidence limits, respectively, provided by LIGO and Virgo Collaboration (Abbott et al. 2018). It is clear that the effect of SRC is to move the $\Lambda_1 \times \Lambda_2$ curves of our excluded volume model to the region of compatibility with the LIGO and Virgo Collaboration data regarding the GW170817 event, due to the fact that SRC decreases the values of both dimensionless tidal deformabilities. In the figure, we also furnish a band with results obtained through the relativistic mean field models studied in (Lourenço et al. 2019) that are consistent with constraints from nuclear matter, pure neutron matter, symmetry energy, and its derivatives analyzed in (Dutra et al. 2014). Notice that the parametrizations of the CCS-SRC model also have a good intersection with this band.

It is also worth to noting that the CCS-SRC parametrizations used to construct Figs. 8, 10, and 11 have the symmetry energy slope at the saturation density around 108 MeV. This value is inside the range of $L_0 = (106 \pm 37) \text{ MeV}$, claimed in Reed et al. (2021) to be in full agreement with the updated results provided by the lead radius experiment (PREX-2) collaboration concerning the neutron skin thickness of ^{208}Pb (Adhikari et al. 2021). Nevertheless, it is also important to mention that there are other stud-

ies pointing out smaller ranges for L_0 . In Reinhard et al. (2021), for instance, the interval of $L_0 = (54 \pm 8)$ MeV was determined from an analysis that takes into account theoretical uncertainties of the parity-violating asymmetry in ^{208}Pb . Ab initio calculations performed in Hu et al. (2022), also for the ^{208}Pb nucleus, predict the range of $L_0 = (37 - 66)$ MeV for the slope parameter. Furthermore, according to Lattimer (2023), the range of $L_0 = (-5 \pm 40)$ MeV is related to the results of the neutron skin thickness of ^{48}Ca provided by CREX Collaboration (Adhikari et al. 2022). Another analysis in Zhang & Chen (2022) combined the results from PREX-2 and CREX and found $L_0 = 15.3^{+46.8}_{-41.5}$ MeV through a Bayesian inference. However, another combination of the PREX-2 and CREX results produced, through a covariance analysis, higher values for this isovector quantity: $L_0 = (82.32 \pm 22.93)$ MeV (Kumar et al. 2023). We verified that for lower values of L_0 , the CCS-SRC parametrizations are not simultaneously compatible with all astrophysical constraints depicted in Fig. 8. Moreover, in this case, the model produces extremely low values of J , for example, $J \sim 19$ MeV for $L_0 = 66$ MeV. This feature leads the bulk parameter space of the model with SRC to the direction of higher values of L_0 . A more complete description, namely, the one in which lower values of L_0 are also allowed, necessarily imposes a suitable modification in the isovector sector. This specific study is already been performed for the CCS-SRC model.

4 SUMMARY AND CONCLUDING REMARKS

In this work, we have included, in a phenomenological way, SRC (Cai & Li 2015, 2016a,b) in a vdW-type model applied to the description of asymmetric nuclear matter. Excluded volume (EV) models have been recently used in relativistic hadronic systems (Vovchenko et al. 2015a,b; Vovchenko 2017; Vovchenko et al. 2017; Sagun et al. 2018). It is an attempt to treat nuclear matter systems more realistically since it considers the nucleon as a finite spatial dimension object and no longer a structureless particle. In (Lourenço et al. 2019; Dutra et al. 2020), in particular, authors developed a density-dependent vdW model in which attractive and repulsive parts of the nucleon-nucleon interaction were assumed depending on the nuclear density. Here we followed the same procedure and have used the Carnahan–Starling method for modeling the latter (see Eq. (7)), and a suitable expression for the former (see Eq. (15)) that ensures the structure of the Clausius real gas model (Vovchenko 2017; Vovchenko et al. 2018). After the implementation of SRC in this theoretical framework, resulting in a model named CCS-SRC (Clausius–Carnahan–Starling–SRC) model, we investigated its capability in correctly describing some features of both, nuclear and stellar matter. The four free parameters of the model are adjusted in order to reproduce saturation density (ρ_0), the binding energy of infinite nuclear matter, incompressibility, and symmetry energy (or symmetry energy slope, equivalently), with all these quantities evaluated at $\rho = \rho_0$.

We verified that one of the effects of including SRC in the model is the shift of the break of causality to a higher-density region. It is important to mention that EV relativistic models suffer from this issue, namely, the break of causality due to the lack of a complete treatment of the Lorentz contraction for the finite-size nucleons. As we have shown, SRC helps to circumvent this problem in an effective way. We also observed that SRC did not destroy the linear relationship between symmetry energy and its slope (L_0), a correlation often found in the literature (Drischler et al. 2020; Li et al. 2021; Santos et al. 2015). Furthermore, SRC increase the value of L_0 in comparison with the model without this phenomenology implemented. At higher density regime, another important finding shown in Fig. 4 is that

the CCS-SRC model completely satisfies the flow constraint, a wide constraint used to validate and select hadronic models (Dutra et al. 2014), for parametrizations constructed by running K_0 in the range of $K_0 = (240 \pm 20)$ MeV (Garg & Colò 2018).

With regard to the stellar matter, the inclusion of SRC in the CCS model softens the EoS generated as input to the TOV equations used to construct the mass-radius profiles. The opposite effect is observed in RMF models presenting quartic self-interaction in the repulsive vector field, namely, models in which the Lagrangian density presents a term given by $C_\omega (\omega^\mu \omega_\mu)^2$. For these models, SRC make the EoS stiffer and consequently capable of producing more massive neutron stars. However, RMF models in which $C_\omega = 0$ exhibit the same behavior as the one found here, i.e., softer EoS in comparison with the ones without SRC added. Nevertheless, the CCS-SRC model still generates mass-radius diagrams compatible with recent astrophysical constraints, such as those coming from gravitational waves data related to the GW170817 (Abbott et al. 2017, 2018) and GW190425 (Abbott et al. 2020) events, data from the NICER mission regarding the pulsars PSR J0030+0451 (Riley et al. 2019; Miller et al. 2019) and PSR J0740+6620 (Riley et al. 2021; Miller et al. 2021); and data from the latter pulsar extracted from Fonseca et al. (2021). Our results show that SRC also favor the model to be consistent with the constraints regarding the dimensionless tidal deformability, namely, the one related to the $1.4M_\odot$, namely, $\Lambda_{1.4} = 190^{+390}_{-120}$ (Abbott et al. 2018), and those from the binary neutron stars system (Abbott et al. 2017), both of them provided by the LIGO and Virgo Collaboration through the analysis of gravitational waves detected in the GW170817 event. In this particular case, it was observed that SRC decrease the value of Λ due to the reduction of the neutron star radius caused by the softening of the EoS.

Finally, the values found for L_0 are inside the range of $L_0 = (106 \pm 37)$ MeV, pointed out in Reed et al. (2021) as compatible with data from the PREX-2 collaboration with regard to the ^{208}Pb neutron skin thickness (Adhikari et al. 2021). We also mention that, for the case in which lower values of L_0 are considered, the model is not able to simultaneously reconcile with all astrophysical constraints. Furthermore, very low values of J are also found in this case. This feature has motivated us to investigate a possible improvement in the isovector sector of the model in order to make it suitable to also reach this particular region of the parameter space.

ACKNOWLEDGMENTS

This work is a part of the project INCT-FNA Proc. No. 464898/2014-5. E. H. R. is supported with a doctorate scholarship by Coordenação de Aperfeiçoamento de Pessoal de Nível Superior (CAPES). This work is also supported by Conselho Nacional de Desenvolvimento Científico e Tecnológico (CNPq) under Grants No. 312410/2020-4 (O.L.) and No. 308528/2021-2 (M.D.). O.L. and M.D. also acknowledge Fundação de Amparo à Pesquisa do Estado de São Paulo (FAPESP) under Thematic Project 2017/05660-0. O. L. is also supported by FAPESP under Grant No. 2022/03575-3 (BPE). This study is also financed by CAPES – Finance Code 001 - Project number 88887.687718/2022-00 (M. D.).

DATA AVAILABILITY STATEMENT

This manuscript has no associated data or the data will not be deposited. All data generated during this study are contained in this published article.

REFERENCES

- Abbott B. P., et al., 2009, *Reports on Progress in Physics*, 72, 076901
- Abbott B. P., Abbott R., Abbott T. D., Acernese F., Ackley K., et al., 2017, *Phys. Rev. Lett.*, 119, 161101
- Abbott B. P., Abbott R., Abbott T. D., Acernese F., Ackley et al., 2018, *Phys. Rev. Lett.*, 121, 161101
- Abbott B. P., Abbott R., Abbott T. D., Abraham S., Acernese F., et al., 2020, *The Astrophysical Journal Letters*, 892, L3
- Accadia T., Acernese F., Alshourbagy M., et al., 2012, *Journal of Instrumentation*, 7, P03012
- Adhikari D., Albataineh H., Androic D., Aniol K., Armstrong D. S., Averett T., et al., 2021, *Phys. Rev. Lett.*, 126, 172502
- Adhikari D., et al., 2022, *Phys. Rev. Lett.*, 129, 042501
- Antoniadis J., et al., 2013, *Science*, 340, 1233232
- Baym G., Pethick C., Sutherland P., 1971, *The Astrophysical Journal*, 170, 299
- Binnington T., Poisson E., 2009, *Phys. Rev. D*, 80, 084018
- Bugaev K. A., 2008, *Nuclear Physics A*, 807, 251
- Bugaev K. A., et al., 2019, *Universe*, 5
- CLAS Collaboration 2018, *Nature*, 560, 617
- CLAS Collaboration 2019, *Nature*, 566, 354
- Cai B.-J., Li B.-A., 2015, *Phys. Rev. C*, 92, 011601
- Cai B.-J., Li B.-A., 2016a, *Phys. Rev. C*, 93, 014619
- Cai B.-J., Li B.-A., 2016b, *Physics Letters B*, 757, 79
- Cai B.-J., Li B.-A., 2022, *Annals of Physics*, 444, 169062
- Camenzind M., 2007, *Compact objects in astrophysics*. Springer
- Carnahan N. F., Starling K. E., 1969, *The Journal of Chemical Physics*, 51, 635
- Damour T., Nagar A., 2010, *Phys. Rev. D*, 81, 084016
- Danielewicz P., Lacey R., Lynch W. G., 2002a, *Science*, 298, 1592
- Danielewicz P., Lacey R., Lynch W. G., 2002b, *Science*, 298, 1592
- Drischler C., Furnstahl R. J., Melendez J. A., Phillips D. R., 2020, *Phys. Rev. Lett.*, 125, 202702
- Duer M., et al., 2019, *Physics Letters B*, 797, 134792
- Dutra M., et al., 2014, *Phys. Rev. C*, 90, 055203
- Dutra M., Santos B. M., Lourenço O., 2020, *Journal of Physics G: Nuclear and Particle Physics*, 47, 035101
- Fonseca E., Cromartie H. T., Pennucci T. T., Ray P. S., et al., 2021, *The Astrophysical Journal Letters*, 915, L12
- Garg U., Colò G., 2018, *Progress in Particle and Nuclear Physics*, 101, 55
- Gendreau K. C., Arzumanyan Z., Adkins P. W., et al., 2016. SPIE, p. 99051H, doi:10.1117/12.2231304, https://doi.org/10.1117/12.2231304
- Gonzalez-Boquera C., Centelles M., Viñas X., Routray T. R., 2019, *Phys. Rev. C*, 100, 015806
- Guo W.-M., Li B.-A., Yong G.-C., 2021, *Phys. Rev. C*, 104, 034603
- Hen O., et al., 2014, *Science*, 346, 614
- Hen O., Miller G. A., Piasetzky E., Weinstein L. B., 2017, *Rev. Mod. Phys.*, 89, 045002
- Hinderer T., 2008, *The Astrophysical Journal*, 677, 1216
- Hu B., et al., 2022, *Nature Physics*, 18, 1196
- Kumar M., Kumar S., Thakur V., Kumar R., Agrawal B. K., Dhiman S. K., 2023, *Phys. Rev. C*, 107, 055801
- LIGO-Caltech 2023, Latest Update on Start of Next Observing Run (O4), https://www.ligo.caltech.edu/news/ligo20220123
- Lalazissis G. A., König J., Ring P., 1997, *Phys. Rev. C*, 55, 540
- Lattimer J. M., 2023, *Particles*, 6, 30
- Li B.-A., Chen L.-W., Ko C. M., 2008, *Physics Reports*, 464, 113
- Li B.-A., Cai B.-J., Xie W.-J., Zhang N.-B., 2021, *Universe*, 7
- Lourenço O., Dutra M., Lenzi C. H., Biswal S. K., Bhuyan M., Menezes D. P., 2020, *European Physical Journal A*, 56, 32
- Lourenço O., Dutra M., Lenzi C. H., Bhuyan M., Biswal S. K., Santos B. M., 2019, *The Astrophysical Journal*, 882, 67
- Lourenço O., Dutra M., Lenzi C. H., Flores C. V., Menezes D. P., 2019, *Phys. Rev. C*, 99, 045202
- Lourenço O., Frederico T., Dutra M., 2022, *Phys. Rev. D*, 105, 023008
- Lourenço O., Lenzi C. H., Frederico T., Dutra M., 2022, *Phys. Rev. D*, 106, 043010
- Menezes D. P., 2021, *Universe*, 7, 267
- Miller M. C., Lamb F. K., Dittmann A. J., Bogdanov S., et al., 2019, *The Astrophysical Journal Letters*, 887, L24
- Miller M. C., Lamb F. K., Dittmann A. J., Bogdanov S., et al., 2021, *The Astrophysical Journal Letters*, 918, L28
- Oppenheimer J. R., Volkoff G. M., 1939, *Phys. Rev.*, 55, 374
- Postnikov S., Prakash M., Lattimer J. M., 2010, *Phys. Rev. D*, 82, 024016
- Reed B. T., Fattoyev F. J., Horowitz C. J., Piekarewicz J., 2021, *Phys. Rev. Lett.*, 126, 172503
- Reinhard P.-G., Roca-Maza X., Nazarewicz W., 2021, *Phys. Rev. Lett.*, 127, 232501
- Riley T. E., Watts A. L., Bogdanov S., Ray P. S., et al., 2019, *The Astrophysical Journal Letters*, 887, L21
- Riley T. E., Watts A. L., Ray P. S., Bogdanov S., et al., 2021, *The Astrophysical Journal Letters*, 918, L27
- Ring P., Schuck P., 2000, *The Nuclear Many-Body Problem*. Springer-Verlag, Berlin
- Sagun V. V., et al., 2018, *European Physical Journal A*, 54, 100
- Santos B. M., Dutra M., Lourenço O., Delfino A., 2015, *Phys. Rev. C*, 92, 015210
- Schmidt A., et al., 2020, *Nature*, 578, 540
- Shlomo S., Kolomietz V. M., Colò G., 2006, *European Physical Journal A*, 30, 23
- Silva J., Lourenço O., Delfino A., Martins J. S., Dutra M., 2008, *Physics Letters B*, 664, 246
- Souza L. A., Dutra M., Lenzi C. H., Lourenço O., 2020, *Phys. Rev. C*, 101, 065202
- Stone J. R., Stone N. J., Moszkowski S. A., 2014, *Phys. Rev. C*, 89, 044316
- Subedi R., et al., 2008, *Science*, 320, 1476
- Tolman R. C., 1939, *Phys. Rev.*, 55, 364
- Tolos L., Centelles M., Ramos A., 2017, *Publications of the Astronomical Society of Australia*, 34, e065
- Vovchenko V., 2017, *Phys. Rev. C*, 96, 015206
- Vovchenko V., Anchishkin D. V., Gorenstein M. I., 2015a, *Journal of Physics A: Mathematical and Theoretical*, 48, 305001
- Vovchenko V., Anchishkin D. V., Gorenstein M. I., 2015b, *Phys. Rev. C*, 91, 064314
- Vovchenko V., Motornenko A., Alba P., Gorenstein M. I., Satarov L. M., Stoecker H., 2017, *Phys. Rev. C*, 96, 045202
- Vovchenko V., Gorenstein M. I., Stoecker H., 2018, *European Physical Journal A*, 54, 16
- Walecka J., 1974, *Annals of Physics*, 83, 491
- Xu J., Chen L.-W., Li B.-A., Ma H.-R., 2009a, *Phys. Rev. C*, 79, 035802
- Xu J., Chen L.-W., Li B.-A., Ma H.-R., 2009b, *The Astrophysical Journal*, 697, 1549
- Zhang Z., Chen L.-W., 2022, Bayesian Inference of the Symmetry Energy and the Neutron Skin in ^{48}Ca and ^{208}Pb from CREX and PREX-2 (arXiv:2207.03328)